

Prospect for measuring work statistics in quantum coherent systems

Cheolhee Han,¹ Nadav Katz,² and Eran Sela³

¹*Department of Data Information and Physics, Kongju National University, Kongju 32588, Republic of Korea*

²*Racah Institute of Physics, the Hebrew University of Jerusalem, Jerusalem 91904, Israel*

³*Raymond and Beverly Sackler School of Physics and Astronomy, Tel Aviv University, Tel Aviv 69978, Israel*

(Dated: March 27, 2025)

Quantum thermodynamics is concerned with heat and work exchange between a quantum coherent system and heat reservoirs or work agents. In stochastic thermodynamics a key object of interest is the statistics of these quantities, but it is notoriously difficult to measure it in general systems. Here we discuss the prospect for measuring work statistics in electronic devices, via a study of a transmon-microcavity system. The microwave cavity acts as a work agent, exchanging work with the transmon. We formulate a protocol to measure the first moments of work $\langle W^n \rangle$ via photon number detection. We find conditions for capturing quantum coherence in the work statistics. Interestingly, by measuring higher moments one can verify the Jarzynski equality $\langle e^{-W/T} \rangle = 1$ including quantum interference. Our work opens a way for measuring work statistics in nontrivial quantum systems.

I. INTRODUCTION

Work statistics is a fundamental object in stochastic thermodynamics, and identifying in it quantum coherence effects has been the subject of intense study. General features of the work distribution function (WDF) have been elucidated in quantum many body systems, ranging from the adiabatic limit of slow driving [1], where the WDF obtains non-Gaussianity, to the opposite limit of quenched quantum many-body systems [2–5], with expected universal behavior in quantum critical systems [6–10], and applications such as Landauer information erasure [11, 12] and information to work conversion particularly using quantum measurements as the fuel for work extraction [13, 14]. The WDF is bound to satisfy non-equilibrium fluctuation theorems [15, 16] such as the Jarzynski equality (JE) [15] and more specific nonequilibrium fluctuation-dissipation-relations [17, 18]. The JE has been verified in numerous classical systems, but in quantum coherent systems its verification remains limited to fully controlled few-level systems [19], while measuring work statistics remains elusive in quantum many-body systems.

To outline the source for this challenge in a particular class of examples, consider a quantum dot system driven by a time dependent gate voltage, which performs work on the electron in the quantum dot. The entire WDF was measured using continuous charge detection [20–24], confirming the Crooks relation [20], JE [23] and nonequilibrium fluctuation-dissipation-relations [24]. Another approach to measure work in quantum dots is via calorimetric measurements [25]. However, quantum coherent effects in quantum dots, involving *e.g.* the Kondo effect, can not be included in the existing work measurement schemes. There are two sources for this limitation: First, the measurement should not disrupt the quantum superposition. To properly define quantum work, the well accepted two-point measurement (TPM) protocol has been introduced [26]. An ingenious method [27, 28] was introduced to measure it using an ancilla qubit, but it can only

be applied in specific well controlled systems. Second, to capture quantum effects, it is needed to confine the entire thermodynamic process to time scales shorter than the coherence time. For quantum dot systems cooled down to $\sim 10\text{mK}$, this requires a $\sim 10^9\text{Hz}$ resolution, which is far beyond the time resolution of current schemes based on charge detection.

Here, we introduce an elementary solid state system, based on a transmon-micro-resonator device, which offers high degree of both coherence and time resolution, as a general platform to measure work statistics in more complicated systems. Previous works already used these coherent devices for thermodynamic purposes and also work extraction [14]. The applicability of our protocol to other systems follows because in our protocol we do not rely on any measurement of this particular system, but rather of the microwave resonator acting as a “quantum work agent”. Its fast operation allows to measure work statistics on short time scales and including quantum coherent effects.

The idea of the quantum work agent [29], which is discussed in detail in this paper, is to consider a dynamic object like a piston that exchanges work with the gas of particles, and measure the work via its own energy change. Here, as the work agent we consider an Harmonic oscillator, particularly an *LC* circuit, whose motion in phase space is not energy conserving due to its interaction with the system, see Fig. 1. Work agents appeared with different names: a first instance, where quantum coherence effects were incorporated in thermodynamic processes [30–32], is the “weight system” [33] having just a gravitational potential and interacting via unitary evolution with the system [34]. Closely related to our work, more recently a harmonic oscillator in the form of a resonator was considered [35] also experimentally [14] as the work agent, also termed a “quantum battery” [36, 37] evolving with the system in an autonomous way, where measurement of its energy fluctuations acts as an embedded quantum work meter. Another term for a similar object is a “quantum flywheel” [38, 39] allowing to mechanically alternate the coupling of a system between a

hot and a cold heat reservoir, which was experimentally realized [40]. Yet, none of these works discussed a general method to measure work statistics in quantum coherent many-body systems, which is our focus here. The distinction between our approach and the one taken in [41] is discussed in Sec. IV.

The outline of the paper is as follows. In Sec. II we present our model and protocol for work measurement. Simulation results are discussed in Sec. III. In Sec. IV we derive the protocol giving an explicit relationship between measured photon number or photon correlations and work moments. In Sec. V we demonstrate that the JE including quantum coherence effects is achieved in the limit of a large photon number. In Sec. VI we conclude with an outlook into nontrivial systems. Important details are relegated to the appendices.

II. MODEL AND PROPOSED EXPERIMENTAL PROTOCOL

We consider a Cooper-pair box (CPB) (or transmon) coupled to a microwave cavity [42]

$$H_{tot} = 4E_c \hat{n}^2 - V_g \hat{n} - E_J \cos \hat{\varphi} + \hbar \omega \hat{a}^\dagger \hat{a} + \hbar \lambda \hat{n} (\hat{a} + \hat{a}^\dagger), \quad (1)$$

where $V_g = 8E_c n_g$. As depicted in Fig. 1, the ‘‘system’’ consists of a Cooper pair box controlled by a charging energy $E_c = \frac{e^2}{2C_\Sigma}$ with $C_\Sigma = C_J + C_g$, and a Josephson energy E_J , having n_g -dependent energy levels $\{E_m\}$. The system is capacitively coupled to the microwave resonator with resonant frequency $\omega = \frac{1}{\sqrt{L_r C_r}}$ with coupling $\hbar \lambda(t > 0) = 2\beta e V_{rms}$, with $\beta = C_g/C_\Sigma$ and $V_{rms} = \sqrt{\hbar \omega / 2C_r}$.

Our target is to measure the work done on the system (CPB without resonator) by a time-dependent external gate voltage, as described by

$$H_{ext}(t) = 4E_c \hat{n}^2 - V_g(t) \hat{n} - E_J \cos \hat{\varphi}, \quad (2)$$

where $V_g = 8E_c n_g(t)$ and $n_g(t) = \bar{n}_g + \delta n_g \cos(\omega t)$. We refer to this as classical driving.

As studied in various quantum dot experiments [20, 21, 23, 24] which were conducted only in the classical regime, the time dependent gate voltage performs work on the system, *i.e.* energy is transferred from the time dependent gate voltage to the system. Here, we want to be able to measure the work, in a way that fully captures and preserves quantum coherence within the system. As reviewed in Sec. IV, the work done by an external time dependent parameter is traditionally defined via the TPM protocol [26], which satisfies the JE but does not have an experimental implementation in general systems. We thus employ the microwave resonator as a dynamic work agent, *i.e.* we simulate the external time dependence of Eq. (2), by the dynamics of Eq. (1).

The thermodynamic process is illustrated in Fig. 2. Initially $\lambda(t < 0) = 0$ and the system is at thermal

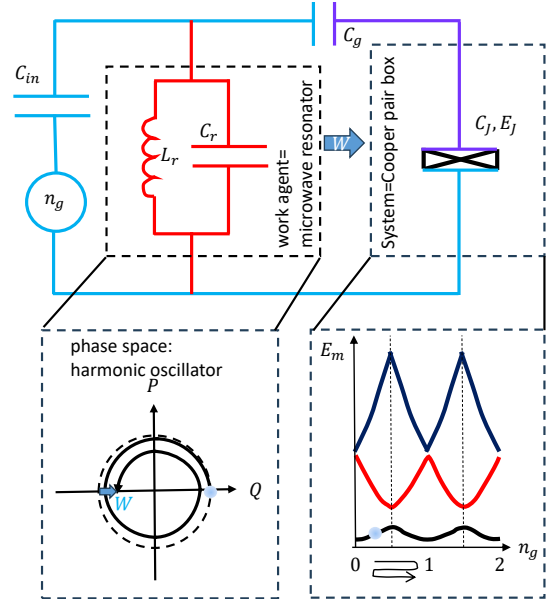


FIG. 1. Cooper-pair box (CPB) coupled to a micro-resonator as a test bed for work statistics measurement and verification of the Jarzynski’s work-fluctuation theorem. The agent is the microwave resonator, which while oscillating exchanges energy with the system - the CPB. The coordinate of the resonator effectively controls the parameter n_g .

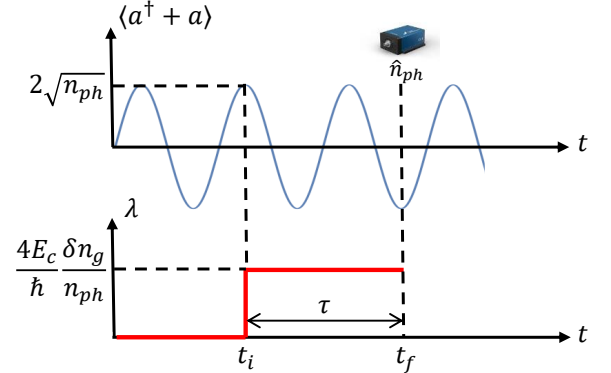


FIG. 2. Three-stage protocol for work measurement: (i) prepare a coherent state in the resonator, initially decoupled from the system which is in a thermal state. (ii) Turn on suddenly the coupling at time t_i . (iii) Measure the photon number in the resonator at time t_f . The average work is obtained using Eq. (4). The second moment is obtained using Eq. (22).

equilibrium at temperature T with $n_{g,initial} = \bar{n}_g + \delta n_g$. While decoupled from the system, the microwave resonator is prepared in a coherent state $\hat{a}|\alpha\rangle = \alpha|\alpha\rangle$ with $\alpha = \sqrt{n_{ph}}$, with $\langle \hat{a} \rangle_t = \sqrt{n_{ph}} e^{-i\omega t}$ and $\langle \hat{a}^\dagger \rangle_t = \sqrt{n_{ph}} e^{i\omega t}$, such that

$$\delta n_g = -\frac{\hbar \lambda}{4E_c} \sqrt{n_{ph}}, \quad (3)$$

where $n_{ph} = \langle \hat{a}^\dagger \hat{a} \rangle_{t=0}$ is the initial average number of photons in the resonator. Then, the coupling λ is turned

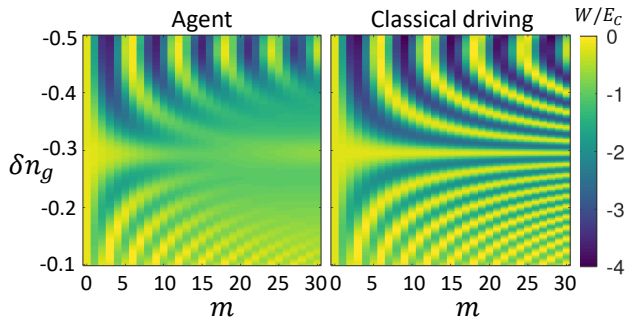


FIG. 3. Average work obtained using the agent protocol (left) or external driving (right) as a function of δn_g and number of periods m , where the total time of the process is $\tau = \frac{\pi(2m+1)}{\omega}$ with integer m . The oscillations stem from Landau-Zener-Stückelberg interference. Here we use $E_C = \hbar\omega$, $E_J = 0.4\hbar\omega$, $T = 0.25\hbar\omega$, and $n_{ph} = 100$. Qualitatively, work is similar to the classical driving.

on at time $t_i = 0$ which is the beginning of the process, where we also suddenly change the gate voltage to $n_{g,final} = \bar{n}$. The process ends at time $t_f = \tau = \frac{\pi(2m+1)}{\omega}$ with some integer m . The photon number is then measured.

Although a more complicated analysis is required to measure higher moments of work (see Sec. IV A), let us first discuss the average work. By energy conservation, the work done by the resonator on the transmon is [14]

$$\langle W \rangle = \hbar\omega(\langle \hat{a}^\dagger \hat{a} \rangle_{t=0} - \langle \hat{a}^\dagger \hat{a} \rangle_{t=\tau}). \quad (4)$$

A simulation of this protocol for a particular set of parameters is shown in the left panel of Fig. 3, for $T = 0.25\hbar\omega$, $E_J = 0.4\hbar\omega$, $E_C = 8\hbar\omega$, $\bar{n}_g = 0.5$ and photon number $n_{ph} = 100$. The resulting $\langle W \rangle$ is plotted both versus δn_g (controlled by λ) and m and displays Landau-Zener-Stückelberg (LZS) interference, as discussed below. The coupling λ varies with δn_g as determined from Eq. (3), and its maximum value is $\lambda = 0.05\omega$. It is compared with the TPM results in the right panel.

When do we expect work statistics extracted from the above protocol to coincide with that of a classical drive $H_{ext}(t)$ using the TPM scheme? We argue that this equivalence occurs for any parameter regime provided the limit $n_{ph} \rightarrow \infty$ is reached. We provide a general argument (yet not a rigorous proof) in Sec. IV, and demonstrate it numerically in various regimes.

Essentially, for a large number of photons, $n_{ph} \gg 1$, the typical work becomes smaller than the energy stored in the oscillator,

$$W_{typical} \ll \hbar\omega n_{ph}. \quad (5)$$

This condition is called the Born-Oppenheimer condition [41]. It is then legitimate to replace \hat{a} and \hat{a}^\dagger in Eq. (1) by their quantum averages.

III. RESULTS

The CPB has various regimes depending on the ratios E_J/E_C , ω/E_J , and δn_g . Our result that work statistics can be accurately extracted using the agent for a large photon number applies in general. Let us discuss two regimes [see Fig. 4]: (i) Landau-Zener regime, in which transitions between energy levels are governed by individual avoided crossings. This occurs for $E_J \ll E_C$ and $\delta n_g \gtrsim 1/2$. An example is in Fig. 3. Here the frequency ω dictates the Landau-Zener transition probability. At the same time we use the agent to measure work, so $\hbar\omega$ is the energy resolution. Nonetheless, our method applies even in the large frequency regime, although this has a price - a type of superresolution.

(ii) Rabi oscillations regime: $E_J \gg E_C$ (transmon limit) or $\delta n_g \ll 1$ where E_m are almost constant. In this regime, it is particularly interesting to consider the resonant case between the agent and the system.

A. Landau-Zener regime and LZS interference

An example of this regime is shown in Fig. 3, which displays LZS oscillations. When an avoided crossing is crossed multiple times due to the oscillating parameter $n_g(t)$, since in each event there is a finite amplitude for an adiabatic passage or for a Landau-Zener transition, there appear interference effects as seen in Fig. 3. But when the parameter $n_g(t)$ is replaced by the work agent coordinate $\propto (\hat{a} + \hat{a}^\dagger)$, the quantum fluctuations of the latter which scales as $\sqrt{n_{ph}}$, can wash out the relative phases. The key question then is: under what conditions, if any, will the dynamic and quantum work agent coherently simulate the process $H_{ext}(t)$? As we explain below and show in detail in Appendix A, the work agent faithfully captures the LZS quantum interference effects provided that

$$\lambda \ll \omega \rightarrow \text{LZS interference.} \quad (6)$$

Crucially, in the $n_{ph} \rightarrow \infty$ limit, keeping δn_g constant we can see from Eq. (3) that this condition will be satisfied. This will be demonstrated numerically in Sec. V.

Let us show the key argument for this inequality. For subsequent analysis, let us consider the lowest pair of levels at $n_g = 1/2$ and define a Pauli matrix $\sigma_z = 1 - 2\hat{n}$. Eq. (1) becomes a two-level system coupled to an harmonic oscillator

$$H_{TLS} = \hbar\lambda \frac{1 - \sigma_z}{2} (\hat{a} + \hat{a}^\dagger) - \frac{E_J}{2} \sigma_x + \hbar\omega \hat{a}^\dagger \hat{a}. \quad (7)$$

The corresponding external Hamiltonian at $\bar{n}_g = 1/2$ is

$$H_{TLS,ext} = -8E_C \delta n_g \cos(\omega t) \frac{1 - \sigma_z}{2} - \frac{E_J}{2} \sigma_x. \quad (8)$$

In order to elucidate the physical origin of the quantum coherence condition, consider $n_g = 1/2$ and let $E_J \ll E_C$ so that energy eigenstates are approximately

σ_z -eigenstates except near the gap closing point (see Fig. 4). The TLS Hamiltonian is controlled by $\text{Re}(\alpha)$ and the transition between $\sigma_z = +1 = \uparrow$ and $\sigma_z = -1 = \downarrow$ occurs upon approaching $\text{Re}(\alpha) = 0$. For $\sigma_z = \uparrow$ the coherent state follows circular trajectories in the complex- α plane centered at $\alpha = 0$, $|\alpha(t)\rangle = |\sqrt{n_{ph}}e^{-i\omega t}\rangle$. For $\sigma_z = \downarrow$ the Harmonic oscillator is shifted and circular motion is centered at $\alpha = -\frac{\lambda}{\omega}$.

Consider an initial state

$$|\Psi(t=0)\rangle = |\uparrow\rangle \otimes |\sqrt{n_{ph}}\rangle. \quad (9)$$

Before it reaches the first Landau-Zener transition, it evolves as $|\Psi(t)\rangle = |\uparrow\rangle \otimes |\sqrt{n_{ph}}e^{-i\omega t}\rangle$. Just after the first Landau-Zener transition we have an entangled system-agent state

$$|\Psi(t)\rangle = \sqrt{P_{LZ}}|\uparrow\rangle \otimes |\sqrt{n_{ph}}e^{-i\omega t}\rangle + \sqrt{1-P_{LZ}}|\downarrow\rangle \otimes |\beta(t)\rangle, \quad (10)$$

where $\beta(t)$ is denoted in Fig. 4 and given by $\beta(t) = -\frac{\lambda}{\omega} + ie^{-i\omega t}(\frac{\lambda}{\omega} + i\sqrt{n_{ph}})$, and P_{LZ} is the Landau-Zener probability. The $\sigma_z = \downarrow$ blob ($\beta(t)$) reaches the next Landau-Zener crossing point $\text{Re}\beta(t) = 0$ at a time Δt after the $\sigma_z = \uparrow$ blob, with $\Delta t \cong \frac{2\lambda}{\omega^2\sqrt{n_{ph}}}$. For times larger than the second Landau-Zener crossing for both blobs, the probability amplitude to find the TLS in the ground state is

$$\langle \uparrow | \Psi(t) \rangle = P_{LZ}|\sqrt{n_{ph}}e^{-i\omega t}\rangle + (1-P_{LZ})|\sqrt{n_{ph}}e^{-i\omega(t+\Delta t)}\rangle. \quad (11)$$

Therefore the corresponding probability $|\langle \uparrow | \Psi(t) \rangle|^2$ contains the interference term $2P_{LZ}(1-P_{LZ})\text{Re}\langle \sqrt{n_{ph}} | \sqrt{n_{ph}} e^{i\omega\Delta t} \rangle$. The overlap between the two coherent states, using the formula $\langle \alpha | \beta \rangle = e^{-\frac{1}{2}|\alpha-\beta|^2}$, is precisely the limiting factor for coherence, and yields Eq. (6).

B. Resonant Work agent and Rabi oscillations

Consider now the regime

$$\hbar\omega \approx E_J \gg \hbar\lambda\sqrt{n_{ph}}, \quad E_J \ll E_c. \quad (12)$$

Now single photons from the resonator can be absorbed or emitted. We further assume that this occurs at the Rabi frequency $\lambda\sqrt{n_{ph}}/2 = 2E_c\delta n_g$, which is much smaller than ω . In the eigenbasis of the E_J -term, the external Hamiltonian maps to the Jaynes-Cummings model (see Appendix C)

$$H_{JC,ext} = \frac{E_J}{2}(|e\rangle\langle e| - |g\rangle\langle g|) - \frac{\hbar\lambda\sqrt{n_{ph}}}{2}(e^{i\omega t}|g\rangle\langle e| + e^{-i\omega t}|e\rangle\langle g|). \quad (13)$$

The work performed by the drive (work agent) on the system coherently oscillates at the Rabi frequency. This is shown in Fig. 5. Comparing the classical driving to the

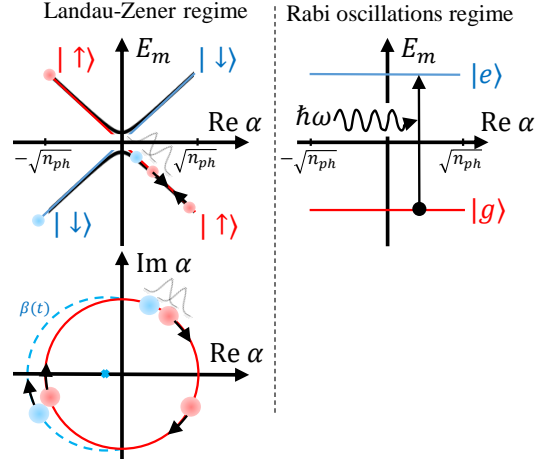


FIG. 4. Landau-Zener regime versus the Rabi oscillations regime. Bottom panel: In the Landau Zener regime, LZS interference is suppressed due to coherent state overlap. The TLS energy splitting is controlled by the coherent state amplitude $\text{Re } \alpha$. The dynamics of the coherent state depends on the TLS state.

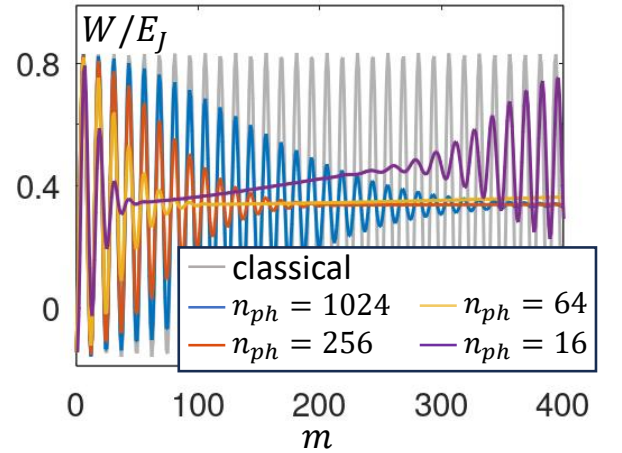


FIG. 5. Work extracted from the work agent in the resonant regime. Comparison between agent with different n_{ph} and classical driving. Here we set $E_C = E_J = \hbar\omega$, $T = 0.01\hbar\omega$, and $\delta n_g = 0.02$. As n_{ph} increases, the decay of the Rabi oscillations is postponed to longer times. For the smallest n_{ph} a revival of the Rabi oscillations is visible.

agent drive we see various effects familiar from quantum optics known as collapse and revival [43]: Here, the coherent oscillations are simply the Rabi oscillations, and in the agent drive the decay occurs due to the dispersion of the Rabi frequency $\sim \lambda/\hbar$. The decay of Rabi oscillations due to the dispersion of the Rabi frequency, for example of a coherent state, is well known experimentally [43], to occur after $\sim \sqrt{n_{ph}}$ Rabi oscillations. Interestingly, the coherent oscillations partially revive after $\sim n_{ph}$ oscillations [43]. As we can see by comparing the classical drive and agent drive in Fig. 5, the two progressively agree up to longer times upon increasing the photon number in

the resonator.

Note that in this resonant regime the typical work is $W_{\text{typical}} \sim \hbar\omega$, requiring to measure a unit change of the number of photons in average using Eq. (4).

IV. GENERAL ARGUMENT FOR THE PROTOCOL

A system is prepared at thermal equilibrium with respect to some Hamiltonian denoted $H_{\text{ext}}(t_i)$, and then evolves as a closed system under the influence of a time dependent Hamiltonian controlled by an external parameter $H_{\text{ext}}(t)$ from $t = t_i$ to $t = t_f$. According to the TPM protocol, the distribution function of the work done on the system by the external parameter is

$$P(W) = \sum_{n_i, n_f} p(n_i) |\langle n_i | U | n_f \rangle|^2 \delta(W - E_{n_f} + E_{n_i}), \quad (14)$$

where p_i is defined as thermal distribution of initial Hamiltonian $H_{\text{ext}}(t_i)$, $p_i = e^{-E_i/T}/Z_i$. $|n_{i/f}\rangle (E_{n_{i/f}})$ is the eigenstate (eigenenergy) of the initial/final Hamiltonian. It follows that

$$\begin{aligned} h(u) &= \int dW P(W) e^{-uW} \\ &= \text{Tr}[e^{-uH_{\text{ext}}(t_f)} U e^{-(\beta-u)H_{\text{ext}}(t_i)} U^\dagger] / Z_i. \end{aligned} \quad (15)$$

$h(u)$ is the generating function of the WDF, allowing to extract the moments from

$$\langle W^n \rangle = \int dW W^n P(W) = (-1)^n \frac{d^n}{du^n} h(u)|_{u \rightarrow 0}. \quad (16)$$

The TPM definition Eq. (14) is consistent with fluctuation theorems and satisfies the JE. We now give a protocol to measure it using a dynamical work agent.

We extend the Hilbert space of the system to include the Hilbert space of a Harmonic oscillator. The total Hamiltonian is $H_{\text{tot}} = H_S + H_a$ with $H_a = \hbar\omega \hat{a}^\dagger \hat{a}$, and the system's Hamiltonian H_S contains the interactions between the system and the agent. Defining a time evolving coherent state $|\alpha(t)\rangle = e^{-iH_a t} |\alpha\rangle$ for a decoupled oscillator, we design the system's Hamiltonian such that

$$\langle \alpha(t) | H_S | \alpha(t) \rangle = H_{\text{ext}}(t). \quad (17)$$

For example, Eq. (1) corresponds to

$$H_{\text{ext}}(t) = 4E_c(\hat{n} - n_g)^2 - E_J \cos \hat{\varphi} + \lambda \hat{n} [\alpha(t) + \alpha(t)^*] \quad (18)$$

where $\alpha(t) = |\alpha| e^{-i\omega t}$. The interaction term corresponds to a shift of n_g , $\delta n_g = -\lambda[\alpha(t) + \alpha(t)^*]/8E_c$.

Eq. (17) has a redundancy with respect to the actual value of $|\alpha|$ since the dynamics only depends on the product $\lambda \cdot |\alpha|$. Denoting the coherent state in terms of its average number of photons, $|\alpha\rangle = |\sqrt{n_{ph}}\rangle$, we will use this

freedom to increase the number of photons while weakening the interaction λ , thus pushing the agent towards the regime $n_{ph} \gg 1$.

This motivates our key mathematical definition of this work,

$$h_a(u) = \text{Tr}[e^{-uH_S} e^{-iH_{\text{tot}} t_f} e^{\frac{u}{2} H_S} \rho_{\text{initial}} e^{\frac{u}{2} H_S} e^{iH_{\text{tot}} t_f}], \quad (19)$$

with the initial density matrix

$$\rho_{\text{initial}} = \frac{e^{-\beta H_{\text{ext}}(t_i)}}{Z_i} \otimes |\sqrt{n_{ph}}\rangle \langle \sqrt{n_{ph}}|. \quad (20)$$

Notice that $\langle \alpha | H_S | \alpha \rangle = H_{\text{ext}}(t_i)$. If we replace the operators \hat{a}^\dagger, \hat{a} by $\alpha(t)^*, \alpha(t)$ in all the factors in Eq. (19), we recover Eq. (15). This replacement is the essence of the Born-Oppenheimer approximation, which in our case becomes justified when the energy stored in the agent well exceeds the typical work done on the system, $\hbar\omega n_{ph} \gg W_{\text{typical}}$. Then, the semiclassical motion of the agent becomes unaffected by the system.

But the Born-Oppenheimer approximation will have corrections for finite n_{ph} , that will be explored below. Notice that while in Eq. (15) the initial state commutes with $H_{\text{ext}}(t_i)$, in Eq. (19) the initial state does not commute with H_S . For this reason we separated the operator e^{uH_S} into two pieces, see Eq. (2) in [44].

With the mathematical definition given in Eq. (19), we now move to the physical protocol. It starts with the preparation of the initial state ρ_{initial} and continues with its evolution according to H_{tot} .

In Ref. [41] it was suggested then to measure the energy of the agent at $t = t_f$ in order to infer the energy change of the system by energy conservation. However the energy measurement of a coherent state suffers from an uncertainty $\propto \sqrt{n_{ph}}$. Minimizing this uncertainty, and also satisfying the Born-Oppenheimer condition, allows access to the WDF only in a limited parameter regime [41].

Here, we formulate a measurement scheme for each work-moment separately using the generating function Eq. (19). We thus avoid the energy uncertainty condition.

A. Moments of the WDF

First moment of work: By applying a u -derivative on Eq. (19), thus dropping a factor of $H_S = H_{\text{tot}} - H_a$ and noticing that H_{tot} commutes with the evolution operator, one readily obtains

$$\langle W \rangle = \hbar\omega \langle \hat{n}_{ph}(t_f) \rangle - \hbar\omega \langle \hat{n}_{ph}(t_i) \rangle. \quad (21)$$

Namely, the average work is obtained, as expected, from an energy measurement of the agent.

Work variance: Higher moments are obtained by applying multiple u -derivatives on Eq. (19). For the second moment one obtains (see Appendix B)

$$\langle W^2 \rangle = (\hbar\omega)^2 [\langle \hat{n}_{ph}^2(t_i) \rangle + \langle \hat{n}_{ph}^2(t_f) \rangle - 2\text{Re}\langle \hat{n}_{ph}(t_f) \hat{n}_{ph}(t_i) \rangle]. \quad (22)$$

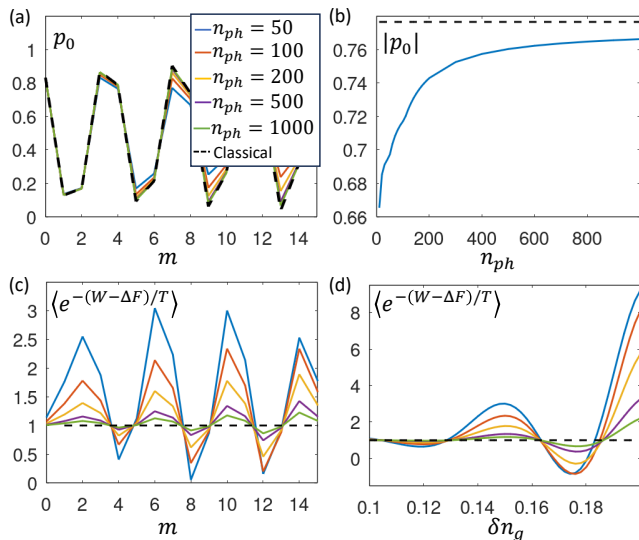


FIG. 6. LZS interference pattern for probability p_0 and $\langle e^{-(W-\Delta F)/T} \rangle$. Here we set $E_C = \hbar\omega$, $T = 0.25\hbar\omega$, $E_J = 0.4\hbar\omega$. (a) p_0 as a function of m , for various n_{ph} ($=50, 100, 200, 500, 1000$) and classical driving. Here we fix $\delta n_g = -0.15$ and vary the number of photons while simultaneously adjusting λ according to Eq. (3). As n_{ph} increases, the interference pattern approaches that of classical driving. (b) The amplitude of the interference as a function of n_{ph} (blue line) and classical driving (black dashed). (c) $\langle e^{-(W-\Delta F)/T} \rangle$ as a function of m with $\delta n_g = 0.15$. (d) $\langle e^{-(W-\Delta F)/T} \rangle$ versus δn_g for $m = 5$.

The first two terms can be extracted, by measuring separately the number distribution function at $t = t_i$ and at $t = t_f$. The most complicated term is two-time correlator in the last term. This can be measured, by preparing instead of a coherent state, a Fock state at $t = t_i$, and then measuring the number distribution at $t = t_f$.

V. TESTING THE JARZYNSKI EQUALITY AND SCALING WITH n_{ph}

So far we argued that our protocol to measure the work and its higher moments, as exemplified for our model in Eq. (1) and (2), is justified under the Born-Oppenheimer condition Eq. (5), which essentially means that the photon number is large enough. Here we test this via the JE. Namely, under the external protocol Eq. (2), the work as defined by the TPM protocol, Eq. (14) identically satisfies $\langle e^{-(W-\Delta F)/T} \rangle = 1$. As we now explicitly demonstrate, the value of $\langle e^{-(W-\Delta F)/T} \rangle$ extracted using our protocol via the agent, approaches unity as the number of photons in the coherent state increases, see Fig. 6.

Let us focus on the TLS. The target WDF is obtained from the external drive in Eq. (2). For this simple model the WDF has three delta-function peaks, $P_{TLS}(W) = p_0\delta(W - W_0) + p_1\delta(W - W_1) + p_2\delta(W - W_2)$. Here, p_0 describes a transition from the ground state to the excited

state, p_1 describes an adiabatic process where the TLS stays in the initial state (either ground or excited state), and p_2 describes the transition probability from the excited state to the ground state. Each one of these probabilities is a product of the probability of the initial state times the transition probability [41]. The eigenenergies of Eq. (8) are $E_{\pm} = -4E_c\delta n_g \pm \sqrt{(4E_c\delta n_g)^2 + (E_J/2)^2}$, hence the energy differences of these three processes upon going from $+\delta n_g$ to $-\delta n_g$ (with $\delta n_g < 0$) are

$$\begin{aligned} W_0 &= E_+(\delta n_g) - E_-(\delta n_g), \\ W_1 &= E_-(\delta n_g) - E_-(\delta n_g) = E_+(\delta n_g) - E_+(\delta n_g), \\ W_2 &= E_-(\delta n_g) - E_+(\delta n_g). \end{aligned} \quad (23)$$

The probability p_0 , as an example, is seen in Fig. 6(a) to nicely compare with the corresponding probability extracted from the dynamical work agent protocol. The approach of the LZS amplitude (the amplitude of the first oscillation) towards the external driving limit is shown in Fig. 6(b) versus n_{ph} .

This comparison between the external drive protocol and the work agent protocol can be tested more strictly via the JE. The WDF $P_{TLS}(W)$ consisting of 3-delta function peaks, by virtue of being defined using the two-time measurement protocol, satisfies the JE. We would like now to test the agent protocol, but the JE probes all moments of the WDF. Hence we will make an approximation. A property of a 3-delta function peak WDF is that it can be fully reconstructed from the first two moments. Indeed from the pair of quantities

$$\begin{aligned} \langle W \rangle &= p_0W_0 + p_1W_1 + p_2W_2, \\ \langle W^2 \rangle &= p_0W_0^2 + p_1W_1^2 + p_2W_2^2, \end{aligned} \quad (24)$$

together with $p_0 + p_1 + p_2 = 1$, all three peaks can be reconstructed. Let us assume that this reconstruction applies for the full WDF of the agent. This is of course an approximation since the delta function peaks are smeared and shifted due to the agent response [41], but this approximation becomes exact in the large limit n_{ph} .

In Fig. 6(c,d) we first evaluate the first and second moments of work. While the first moment is obtained from the average photon number, Eq. (4), the second moment requires photon correlations of the agent, using Eq. (22). We compute these correlations in our simulation. Then, using the above reconstruction of the WDF, we evaluate $\langle e^{-(W-\Delta F)/T} \rangle$. This particular combination of all the moments should not display any interference and is fixed to unity, see dashed lines. The observed oscillations reflect an error of the agent measurement protocol. However, this error diminishes upon increasing the photon number in the agent's coherent state, in accordance with the Born-Oppenheimer condition.

VI. SUMMARY AND OUTLOOK

We developed the concept of the dynamical work agent to measure work statistics. We generalized our recent

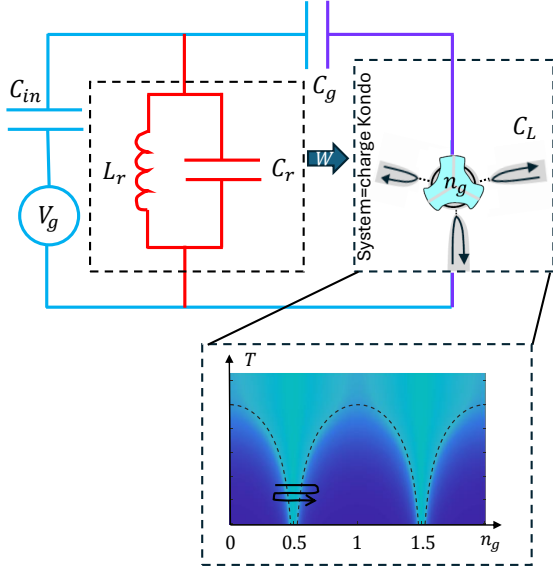


FIG. 7. Hybrid quantum dot-microresonator system: we replace the qubit Josephson junction by a metallic quantum dot connected to M (here $M = 3$) leads realizing the M -channel Kondo critical state. Sweeping the gate voltage n_g on the GHz regime allows to probe work statistics with nontrivial Kibble-Zurek scaling regimes using Eq. (4).

approach [41], in which work statistics is obtained solely from energy measurements of the agent, which is limited by energy uncertainty, and instead here we designed particular observables of the agent whose measured quantum average coincides with a desired momentum of the work distribution. This moment-specific approach is similar to one taken recently for the measurement of entanglement entropy in mesoscopic systems from charge detection [45].

Using this approach, we theoretically demonstrated the possibility of measuring work statistics on the GHz scale by focusing on a Cooper pair box (transmon) coupled to a microwave resonator. In this system we captured quantum coherent effects such as Landau-Zener-Stückelberg interference or Rabi oscillations and their collapse and revival. The particular model Hamiltonian we studied, however, is trivial, and was selected as a proof of concept. A key motivation for an experimental demonstration of our protocol is to open the door to explore the work statistics in nontrivial systems.

One possibility is to consider many-body physics in Josephson junction arrays, see *e.g.* Ref. [46]. Alternatively, in Fig. 7 we envision a hybrid quantum dot-microresonator system. Experiments demonstrating the coupling of double quantum dots to microwave resonators have been demonstrated [47–50] including in the strong coupling limit [51–53]. While there quantum dots behaves just like two level systems, let us consider a quan-

tum dot displaying nontrivial physics. Fig. 7 we display a metallic quantum dot realizing the charge Kondo effect [54–56], which is, for the case of more than one lead, a quantum critical point hosting exotic anyonic excitations with nontrivial thermodynamic entropy [57–59]. In this system, the gate voltage n_g acts as a tuning parameter of the quantum critical point. Recently, exact results appeared for the work statistics of this family of quantum critical point [60]. The nontrivial regimes enter for time scales $\tau \sim \frac{\hbar}{k_B T} \sim 10^{-9}$ sec. Thus combining the quantum dot gate with a microwave resonator could be a promising route to explore the strong non-equilibrium and quantum regimes in stochastic thermodynamics.

ACKNOWLEDGMENTS

We thank discussions with Doron Cohen. ES gratefully acknowledges support from the European Research Council (ERC) under the European Union Horizon 2020 research and innovation program under grant agreement No. 951541. This work was supported by the research grant of Kongju National University in 2024.

Appendix A: LZS interference

We consider H_{TLS} of Eq. (7) at $n_g = 1/2$. Our initial state is $|\uparrow\rangle \otimes |\sqrt{n_{ph}}\rangle$ and we are interested at the evolved state at specific time $\tau_m = \frac{(2m+1)\pi}{\hbar\omega}$. For this purpose it is convenient to rewrite Eq. (7) as $H_{TLS} = H_0 + H_{EJ}$ where

$$\begin{aligned} H_0 &= H_\uparrow \otimes |\uparrow\rangle\langle\uparrow| + H_\downarrow \otimes |\downarrow\rangle\langle\downarrow|, \\ H_{EJ} &= -\frac{E_J}{2} I \otimes (|\uparrow\rangle\langle\downarrow| + |\downarrow\rangle\langle\uparrow|), \end{aligned} \quad (\text{A1})$$

and the operators $H_{\uparrow,\downarrow}$ act only on the agent,

$$\begin{aligned} H_\uparrow &= \hbar\omega \hat{a}^\dagger \hat{a}, \\ H_\downarrow &= \hbar\omega \left(\hat{a}^\dagger + \frac{\lambda}{\omega} \right) \left(\hat{a} + \frac{\lambda}{\omega} \right) - \frac{\hbar\lambda^2}{\omega}. \end{aligned} \quad (\text{A2})$$

Let us expand the evolution operator from t_i to t_f , with $t_f - t_i = \tau = \frac{\pi(2m+1)}{\omega}$, up to first order in E_J . Defining the unperturbed propagator as $U_0(t_2, t_1) = \exp(-iH_0(t_2 - t_1)/\hbar)$, we have

$$\begin{aligned} U(\tau, 0) &= e^{-iH_{TLS}\tau/\hbar} \\ &\simeq U_0(\tau, 0) - \frac{i}{\hbar} \int_0^\tau dt_1 U_0(\tau, t_1) H_{EJ} U_0(t_1, 0) + \dots \end{aligned} \quad (\text{A3})$$

The evolved state becomes

$$|\psi(t_f)\rangle = |-\sqrt{n_{ph}}\rangle|\uparrow\rangle + \frac{iE_J}{2\hbar} \int_0^\tau dt e^{-iH_\downarrow(\tau-t)} |\sqrt{n_{ph}}e^{-i\omega t}\rangle|\downarrow\rangle + \dots \quad (\text{A5})$$

Up to second order in E_J , the probability to find the system in state $|\downarrow\rangle$ (namely the ground state) at t_f is given by

$$\begin{aligned} P_\downarrow &= |\langle\downarrow|\psi(t_f)\rangle|^2 = (E_J/2\hbar)^2 \mathcal{I}, \\ \mathcal{I} &= \int_0^\tau dt_1 \int_0^\tau dt_2 \langle\sqrt{n_{ph}}| e^{iH_\uparrow t_2/\hbar} e^{iH_\downarrow(t_1-t_2)/\hbar} e^{-iH_\uparrow t_1/\hbar} |\sqrt{n_{ph}}\rangle. \end{aligned} \quad (\text{A6})$$

For each pair (t_1, t_2) , this is the overlap between the two paths in which the spin occurs at times t_1 and t_2 , respectively.

To compute the double integral, we define the shifted operator $\hat{a}_\downarrow = \hat{a} + \frac{\lambda}{\omega}$ and note that its coherent state, satisfying $\hat{a}_\downarrow|\alpha\rangle_\downarrow = \alpha|\alpha\rangle_\downarrow$, is proportional to a coherent state of \hat{a} ,

$$|\alpha\rangle = e^{-i\frac{\lambda}{\omega}\text{Im}[\alpha]} |\alpha + \frac{\lambda}{\omega}\rangle_\downarrow, \quad (\text{A7})$$

To see this, we note that the coherent state $|\alpha\rangle$ of \hat{a} must be proportional to $|\alpha + \frac{\lambda}{\omega}\rangle_\downarrow$, but there is an additional phase factor. To obtain the additional phase factor, we compute the overlap $\langle\downarrow|\alpha + \frac{\lambda}{\omega}\rangle_\downarrow$. $|\alpha\rangle$ is written as

$$|\alpha\rangle = e^{-\frac{|\alpha|^2}{2}} \sum_{k=0}^{\infty} \frac{\alpha^k}{k!} (\hat{a}^\dagger)^k |0\rangle. \quad (\text{A8})$$

Using $|0\rangle = |\frac{\lambda}{\omega}\rangle_\downarrow$, then

$$e^{-\frac{|\alpha|^2}{2}} \sum_{k=0}^{\infty} \frac{\alpha^k}{k!} (a_\downarrow^\dagger - \frac{\lambda}{\omega})^k |\frac{\lambda}{\omega}\rangle_\downarrow. \quad (\text{A9})$$

Then the overlap is

$$\begin{aligned} \langle\downarrow|\alpha + \frac{\lambda}{\omega}\rangle_\downarrow &= e^{-\frac{|\alpha|^2}{2}} \sum_{k=0}^{\infty} \langle\downarrow|\alpha + \frac{\lambda}{\omega}\rangle_\downarrow \frac{\alpha^k}{k!} (a_\downarrow^\dagger - \frac{\lambda}{\omega})^k |\frac{\lambda}{\omega}\rangle_\downarrow = e^{-\frac{|\alpha|^2}{2}} \sum_{k=0}^{\infty} \langle\downarrow|\alpha + \frac{\lambda}{\omega}\rangle_\downarrow \frac{|\alpha|^{2k}}{k!} \\ &= e^{\frac{|\alpha|^2}{2}} e^{-\frac{1}{2}|\alpha + \frac{\lambda}{\omega}|^2 - \frac{1}{2}\frac{\lambda^2}{\omega^2} + (\alpha^* + \frac{\lambda}{\omega})\frac{\lambda}{\omega}} = e^{-i\frac{\lambda}{\omega}\text{Im}[\alpha]}, \end{aligned} \quad (\text{A10})$$

with the desired phase factor in Eq. (A7).

It follows that

$$\begin{aligned} &e^{-iH_\downarrow(\tau-t)} |\sqrt{n_{ph}}e^{-i\omega t}\rangle|\downarrow\rangle \\ &= e^{-iH_\downarrow(\tau-t)} e^{i\frac{\lambda}{\omega}\sqrt{n_{ph}}\sin(\omega t)} |\sqrt{n_{ph}}e^{-i\omega t} + \frac{\lambda}{\omega}\rangle_\downarrow|\downarrow\rangle \\ &= e^{i\frac{\lambda}{\omega}\sqrt{n_{ph}}\sin(\omega t)} e^{i\frac{\lambda^2}{\omega^2}(\tau-t)} |(\sqrt{n_{ph}}e^{-i\omega t} + \frac{\lambda}{\omega})e^{-i\omega(\tau-t)}\rangle_\downarrow|\downarrow\rangle, \end{aligned} \quad (\text{A11})$$

giving

$$\begin{aligned} \mathcal{I} &= \int_0^{\frac{(2m+1)\pi}{\hbar\omega}} dt_1 dt_2 \langle-\sqrt{n_{ph}} - \frac{\lambda}{\omega}e^{i\omega t_2} | -\sqrt{n_{ph}} - \frac{\lambda}{\omega}e^{i\omega t_1}\rangle_\downarrow e^{i\frac{\lambda}{\omega}\sqrt{n_{ph}}(\sin(\omega t_1) - \sin(\omega t_2))} e^{i\frac{\lambda^2}{\hbar\omega}(t_2 - t_1)} \\ &= \int_0^{\frac{(2m+1)\pi}{\hbar\omega}} dt_1 dt_2 e^{i\frac{\lambda^2}{\omega}(t_2 - t_1) - \frac{\lambda^2}{\omega^2}(1 - e^{i\omega(t_1 - t_2)})} e^{-\frac{2\lambda\sqrt{n_{ph}}}{\omega}i(\sin(\omega t_2) - \sin(\omega t_1))}. \end{aligned} \quad (\text{A12})$$

The resulting Eq. (A12) is the starting point of the remaining calculations in this section. While it can be calculated exactly, see Eq. (A23), we first would like to understand few limits from this integral.

1. Classical limit

First consider the classical limit $\lambda \rightarrow 0$ with $n_{ph} \rightarrow \infty$, such that $\lambda\sqrt{n_{ph}}/\omega \rightarrow$ finite constant, in which $\hat{a} + \hat{a}^\dagger$ describes a purely external time dependent parameter. Then the double integral in Eq. (A12) becomes the absolute value squared of a single integral, which itself describes the total quantum amplitude,

$$\mathcal{I}_{\substack{\lambda \rightarrow 0 \\ \lambda\sqrt{n_{ph}}/\omega \rightarrow \text{finite}}} = \left| \int_0^{\frac{(2m+1)\pi}{\hbar\omega}} dt_1 e^{i\frac{2\lambda\sqrt{n_{ph}}}{\omega} \sin(\omega t_1)} \right|^2. \quad (\text{A13})$$

For simplicity, let us assume that $\lambda\sqrt{n_{ph}}$ is very large which allows us to evaluate this integral saddle-point approximation.

First, for $m = 0$, we obtain

$$\int_0^{\frac{\pi}{\hbar\omega}} dt_1 e^{i\frac{2\lambda\sqrt{n_{ph}}}{\omega} \sin(\omega t_1)} \simeq \int_{-\infty}^{\infty} dt_1 e^{i\frac{2\lambda\sqrt{n_{ph}}}{\omega} (1 - \frac{1}{2}\omega^2 t_1^2)} = e^{i\frac{2\lambda\sqrt{n_{ph}}}{\omega}} \sqrt{\frac{\pi}{i\lambda\sqrt{n_{ph}}\omega}}. \quad (\text{A14})$$

The phase $e^{i\frac{2\lambda\sqrt{n_{ph}}}{\omega}}$ corresponds to the dynamical phase accumulated from $t = \frac{\pi}{2\hbar\omega}$ to $\frac{\pi}{\hbar\omega}$. This indicates that the spin flip occurs around $t = \frac{\pi}{2\hbar\omega}$, when the gap is the smallest.

After taking the absolute square of the integral, we obtain the probability $P_\downarrow = \frac{\pi E_J^2}{4\hbar^2 \lambda \omega \sqrt{n_{ph}}}$, which coincides with the limit $E_J \rightarrow 0$ of the Landau-Zener probability $P_\downarrow = 1 - e^{-\frac{\pi E_J^2}{2\hbar^2 \lambda \omega \sqrt{n_{ph}}}}$.

Next, consider $m \neq 0$. The $\sin(\omega t_1)$ in the argument of the exponential in Eq. (A13) has $m + 1$ maxima and m minima. Treating these extreme via the saddle-point approximation, we have

$$\begin{aligned} \int_0^{\frac{(2m+1)\pi}{\hbar\omega}} dt_1 e^{i\frac{2\lambda\sqrt{n_{ph}}}{\omega} \sin(\omega t_1)} &\simeq (m+1) \int_{-\infty}^{\infty} dt_1 e^{i\frac{2\lambda\sqrt{n_{ph}}}{\omega} (1 - \frac{1}{2}\omega^2 t_1^2)} + m \int_{-\infty}^{\infty} dt_1 e^{-i\frac{2\lambda\sqrt{n_{ph}}}{\omega} (1 - \frac{1}{2}\omega^2 t_1^2)} \\ &= (m+1) e^{i\frac{2\lambda\sqrt{n_{ph}}}{\omega}} \sqrt{\frac{\pi}{i\lambda\sqrt{n_{ph}}\omega}} + m e^{-i\frac{2\lambda\sqrt{n_{ph}}}{\omega}} \sqrt{\frac{\pi}{-i\lambda\sqrt{n_{ph}}\omega}}. \end{aligned} \quad (\text{A15})$$

Note that the phase $e^{i\frac{2\lambda\sqrt{n_{ph}}}{\omega}}$ is the dynamical phase accumulated from $t = \frac{\pi}{2\omega}(4n+1)$ ($n = 0, 1, 2, \dots, m$) to $t = \frac{\pi}{\omega}(2m+1)$ and $e^{-i\frac{2\lambda\sqrt{n_{ph}}}{\omega}}$ is the dynamical phase accumulated from $t = \frac{\pi}{2\omega}(4n+3)$ to $t = \frac{\pi}{\omega}(2m+1)$. Taking the absolute value squared of this equation, we obtain

$$\mathcal{I} = \frac{\pi}{\lambda\sqrt{n_{ph}}\omega} \left[(2m^2 + 2m + 1) - 2m(m+1) \sin \frac{4\lambda\sqrt{n_{ph}}}{\omega} \right]. \quad (\text{A16})$$

We can inspect oscillations versus n_{ph} , due to dynamical phase, however there is no oscillation versus m . This result is plotted in Fig. 3, and compared with the full simulation.

2. Agent driving

Now we compute Eq. (A12) for finite λ and finite n_{ph} , and study the deviation from the classical limit. To compute the integral, we expand it as a power series in λ/ω ,

$$\mathcal{I} = \sum_{n=0}^{\infty} \frac{1}{n!} \frac{\lambda^{2n}}{\omega^{2n}} e^{-\frac{\lambda^2}{\omega^2}} \int_0^{\frac{(2m+1)\pi}{\omega}} dt_1 dt_2 e^{i\frac{\lambda^2}{\omega}(t_2-t_1)} e^{in\omega(t_1-t_2)} e^{-\frac{2\sqrt{n_{ph}}\lambda}{\omega} i(\sin(\omega t_2) - \sin(\omega t_1))}. \quad (\text{A17})$$

The double integral in Eq. (A12) is now a sum over a products of two independent integrals of the form

$$\int_0^{(2m+1)\frac{\pi}{\hbar\omega}} dt_1 e^{i(n\omega - \frac{\lambda^2}{\omega})t_1 + i\frac{2\lambda\sqrt{n_{ph}}}{\omega} \sin(\omega t_1)} \int_0^{(2m+1)\frac{\pi}{\omega}} dt_2 e^{-i(n\omega - \frac{\lambda^2}{\omega})t_2 - i\frac{2\lambda\sqrt{n_{ph}}}{\omega} \sin(\omega t_2)}. \quad (\text{A18})$$

Before performing the integral explicitly, let us again apply the saddle-point approximation by assuming that $\lambda\sqrt{n_{ph}}$ is large. The first integrand can be written as $e^{f(t)}$ with

$$\begin{aligned} f(t_1) &= i(n\omega - \frac{\lambda^2}{\omega})t_1 + i\frac{2\lambda\sqrt{n_{ph}}}{\omega} \sin(\omega t_1), \\ \partial_{t_1} f(t_1) &= i(n\omega - \frac{\lambda^2}{\omega}) + i2\lambda\sqrt{n_{ph}} \cos(\omega t_1) = 0. \end{aligned} \quad (\text{A19})$$

Now $f(t_1)$ has extrema at approximately $t_{1,0} \simeq \frac{\pi(4p+1)}{2\omega} + \frac{n - \frac{\lambda^2}{(h\omega)^2}}{2\lambda\sqrt{n_{ph}}}$ and $\frac{\pi(4q+3)}{2\omega} - \frac{n - \frac{\lambda^2}{(h\omega)^2}}{2\lambda\sqrt{n_{ph}}}$, where p (q) is an integer number smaller than m ($m-1$). These points correspond to the avoided crossings, up to small corrections $\propto \frac{1}{\sqrt{n_{ph}}}$, which signal small deviations from the Born-Oppenheimer condition. In this case the trajectory of the agent is weakly affected by the spin-flips occurring in the system. Then the last integral becomes

$$\begin{aligned} \int_0^{(2m+1)\frac{\pi}{h\omega}} dt_1 e^{i(n\omega - \frac{\lambda^2}{\omega})t_1 + i\frac{2\lambda\sqrt{n_{ph}}}{\omega} \sin(\omega t_1)} &\simeq \sum_{p=0}^m e^{i(n\omega - \frac{\lambda^2}{h^2\omega})(\frac{\pi(4p+1)}{2\omega} + \frac{n - \frac{\lambda^2}{(h\omega)^2}}{2\lambda\sqrt{n_{ph}}})} e^{i\frac{2\lambda\sqrt{n_{ph}}}{\omega}} e^{-i\frac{1}{2}\omega\frac{(n - \frac{\lambda^2}{\omega^2})^2}{2\lambda\sqrt{n_{ph}}}} \int_{-\infty}^{\infty} d\delta t_1 e^{-i\frac{1}{2}2\lambda\sqrt{n_{ph}}\omega\delta t_1^2} \\ &+ \sum_{q=0}^{m-1} e^{i(n\omega - \frac{\lambda^2}{\omega})(\frac{\pi(4q+3)}{2\omega} - \frac{n - \frac{\lambda^2}{(h\omega)^2}}{2\lambda\sqrt{n_{ph}}})} e^{-i\frac{2\lambda\sqrt{n_{ph}}}{h\omega}} e^{i\frac{1}{2}\omega\frac{(n - \frac{\lambda^2}{\omega^2})^2}{2\lambda\sqrt{n_{ph}}}} \int_{-\infty}^{\infty} d\delta t_1 e^{i\frac{1}{2}2\lambda\sqrt{n_{ph}}\omega\delta t_1^2}. \end{aligned} \quad (\text{A20})$$

Skipping the calculation of the Gaussian integral and summation over m , we finally obtain

$$\begin{aligned} \mathcal{I} &\simeq \frac{\pi e^{-\frac{\lambda^2}{\omega^2}}}{\lambda\omega\sqrt{n_{ph}}} \sum_{n=0}^{\infty} \left[\frac{\sin^2(\pi(m+1)(n - \frac{\lambda^2}{\omega^2}))}{\sin^2(\pi(n - \frac{\lambda^2}{\omega^2}))} + \frac{\sin^2(\pi m(n - \frac{\lambda^2}{\omega^2}))}{\sin^2(\pi(n - \frac{\lambda^2}{\omega^2}))} \right. \\ &\quad \left. + 2\sin\left(\frac{\lambda\sqrt{n_{ph}}}{\omega} + \omega\frac{(n - \frac{\lambda^2}{\omega^2})^2}{2\lambda\sqrt{n_{ph}}}\right) \frac{\sin(\pi(m+1)(n - \frac{\lambda^2}{\omega^2}))\sin(\pi m(n - \frac{\lambda^2}{\omega^2}))}{\sin^2(\pi(n - \frac{\lambda^2}{\omega^2}))} \right] \\ &\simeq \frac{\pi}{2\lambda\omega\sqrt{n_{ph}} \sin^2\left(\frac{\pi\lambda^2}{\omega^2}\right)} \left[2e^{-\frac{2\lambda^2}{\omega^2}} \sin\left(\frac{\sqrt{n_{ph}}\lambda}{\omega}\right) \left(\cos\left(\frac{\pi\lambda^2}{\omega^2}\right) - \cos\left(\frac{\pi\lambda^2(2m+1)}{\omega^2}\right) \right) \right. \\ &\quad \left. + 2 - \cos\left(\frac{2\pi\lambda^2(m+1)}{\omega^2}\right) - \cos\left(\frac{2\pi\lambda^2 m}{\omega^2}\right) \right]. \end{aligned} \quad (\text{A21})$$

As opposed to the classical driving case Eq. (A16), here there are oscillations versus m . As far as the goal of reproducing the classical driving using the agent is concerned, these oscillations are an artifact of the correction to the dynamical phase coming from the deviations from the Born-Oppenheimer condition. We can see that the relative size of these corrections is $\mathcal{O}\left(\frac{\lambda^2}{\omega^2}\right)$.

3. Exact evaluation of (A12)

Using the expansion in Eq. (A17), the integral is computed as

$$\mathcal{I} = \frac{\pi^2}{\omega^2} \left| \frac{\sin(\pi(n - \frac{\lambda^2}{\omega^2})(m+1))}{\sin(\pi(n - \frac{\lambda^2}{\omega^2}))} \Phi_{-n + \frac{\lambda^2}{\omega^2}}^*(x) + \frac{\sin(\pi(n - \frac{\lambda^2}{\omega^2})m)}{\sin(\pi(n - \frac{\lambda^2}{\omega^2}))} \Phi_{n - \frac{\lambda^2}{\omega^2}}(x) \right|^2, \quad (\text{A22})$$

where $x = 2\lambda\sqrt{n_{ph}}/\omega$ and $\Phi_\nu(x) = J_\nu(x) + iE_\nu(x)$, where $J_\nu(x)$ is the Anger function and $E_\nu(x)$ is the Weber function. Then the integral in Eq. (A12) becomes

$$\mathcal{I} = e^{-\frac{\lambda^2}{\omega^2}} \sum_{n=0}^{\infty} \frac{1}{n!} \frac{\lambda^{2n}}{\omega^{2n}} \frac{\pi^2}{\omega^2} \left| \frac{\sin(\pi(n - \frac{\lambda^2}{\omega^2})(m+1))}{\sin(\pi(n - \frac{\lambda^2}{\omega^2}))} \Phi_{-n + \frac{\lambda^2}{\omega^2}}^*(x) + \frac{\sin(\pi(n - \frac{\lambda^2}{\omega^2})m)}{\sin(\pi(n - \frac{\lambda^2}{\omega^2}))} \Phi_{n - \frac{\lambda^2}{\omega^2}}(x) \right|^2. \quad (\text{A23})$$

As explained above, note that the probability contains oscillations both versus m and n_{ph} . In the limit of classical driving ($\lambda \rightarrow 0$), the oscillation of m disappears and becomes a quadratic function, see Eq. (A16). This perturbative expression in E_J nicely compares with the simulation of the full model as displayed in Fig. 8.

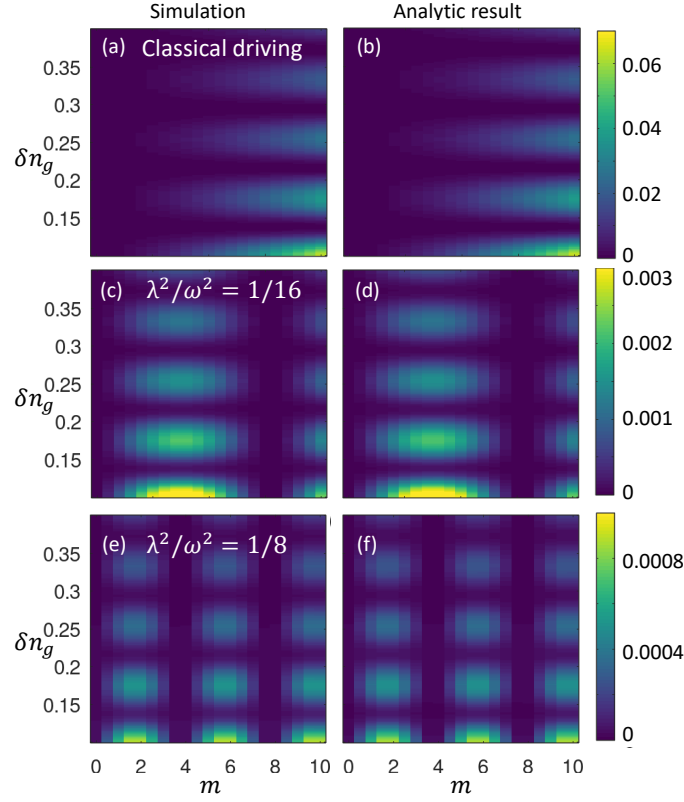


FIG. 8. Transition probability P_d for various λ/ω . Here we set $E_C = \hbar\omega$ and $E_J = 0.01\hbar\omega$, where the perturbative calculation is applicable. The plots in the right column are obtained from Eq. (A23).

Appendix B: First moments of WDF from correlations of $a^\dagger a$

Here we derive general expressions for moments of the work distribution function in terms of multi-point correlators of the photon number $\hat{n}_{ph}(t) = e^{iH_{tot}t}\hat{n}_{ph}e^{-iH_{tot}t}$. We first define the system's Hamiltonian

$$H_S(t) = H_{tot} - H_a(t) \quad (B1)$$

and use it to define a new generating function corresponding to Eq. (15),

$$h_a(u) = \text{Tr}[e^{\frac{u}{2}H_S}\rho e^{\frac{u}{2}H_S}e^{iH_{tot}t_f}e^{-uH_S}e^{-iH_{tot}t_f}]. \quad (B2)$$

Explicitly,

$$h_a(u) = \text{Tr}[e^{\frac{u}{2}(H_{tot}-\omega\hat{n}_{ph})}\rho e^{\frac{u}{2}(H_{tot}-\omega\hat{n}_{ph})}e^{iH_{tot}t_f}e^{-u(H_{tot}-\omega\hat{n}_{ph})}e^{-iH_{tot}t_f}]. \quad (B3)$$

To obtain work, we take the derivative of u and $u \rightarrow 0$. Then we obtain

$$W = \omega\langle\hat{n}_{ph}(t_f)\rangle - \omega\langle\hat{n}_{ph}(t_i)\rangle \quad (B4)$$

To obtain higher moments, we use Zassenhaus formula, which is

$$\begin{aligned} e^{\frac{u}{2}(H_{tot}-\omega\hat{n}_{ph})} &= e^{\frac{u}{2}H_{tot}}e^{-\frac{u}{2}\omega\hat{n}_{ph}}e^{-\frac{u^2}{8}[H_{tot},\omega\hat{n}_{ph}]} \times e^{\mathcal{O}(u^3)} \\ &= e^{-\frac{u^2}{8}[\omega\hat{n}_{ph},H_{tot}]}e^{-\frac{u}{2}\omega\hat{n}_{ph}}e^{\frac{u}{2}H_{tot}} \times e^{\mathcal{O}(u^3)}. \end{aligned} \quad (B5)$$

Put this into the generating function, then

$$\begin{aligned} h_a(u) &= \text{Tr}[e^{\frac{u}{2}H_{tot}}e^{-\frac{u}{2}\omega\hat{n}_{ph}}e^{\frac{u^2}{8}[H_{tot},\omega\hat{n}_{ph}]}e^{\mathcal{O}(u^3)}\rho e^{\mathcal{O}(u^3)}e^{-\frac{u^2}{8}[\omega\hat{n}_{ph},H_{tot}]} \\ &\quad \times e^{-\frac{u}{2}\omega\hat{n}_{ph}}e^{\frac{u}{2}H_{tot}}e^{iH_{tot}t_f}e^{-\frac{u}{2}H_{tot}}e^{\frac{u}{2}\omega\hat{n}_{ph}}e^{\mathcal{O}(u^3)}e^{\frac{u}{2}\omega\hat{n}_{ph}}e^{-\frac{u}{2}H_{tot}}e^{-iH_{tot}t_f}] \\ &= \text{Tr}[e^{-\frac{u}{2}\omega\hat{n}_{ph}}e^{\frac{u^2}{8}[H_{tot},\omega\hat{n}_{ph}]}e^{\mathcal{O}(u^3)}\rho e^{\mathcal{O}(u^3)}e^{-\frac{u^2}{8}[\omega\hat{n}_{ph},H_{tot}]}e^{-\frac{u}{2}\omega\hat{n}_{ph}}e^{iH_{tot}t_f}e^{\frac{u}{2}\omega\hat{n}_{ph}}e^{\mathcal{O}(u^3)}e^{\frac{u}{2}\omega\hat{n}_{ph}}e^{-iH_{tot}t_f}] \end{aligned} \quad (B6)$$

By taking derivative of u twice and $u \rightarrow 0$, we obtain the variance of the work,

$$\begin{aligned} W^2 &= \omega^2 \text{Tr}[\rho \hat{n}_{ph}^2] + \omega^2 \text{Tr}[\rho e^{iH_{tot}t_f} \hat{n}_{ph}^2 e^{-iH_{tot}t_f}] - \omega^2 \text{Tr}[\rho e^{iH_{tot}t_f} \hat{n}_{ph} e^{-iH_{tot}t_f} \hat{n}_{ph}] - \omega^2 \text{Tr}[\rho \hat{n}_{ph} e^{iH_{tot}t_f} \hat{n}_{ph} e^{-iH_{tot}t_f}] \\ &= \omega^2 \langle \hat{n}_{ph}^2(t_i) \rangle + \omega^2 \langle \hat{n}_{ph}^2(t_f) \rangle - 2\omega^2 \text{Re}[\langle \hat{n}_{ph}(t_f) \hat{n}_{ph}(t_i) \rangle]. \end{aligned} \quad (\text{B7})$$

To obtain higher moments, consider more orders of the Zassenhaus formula.

Appendix C: Relation to decay and revivals of Rabi oscillations

The ground and excited states of H_{TLS} at $n_g = 1/2$ are $|g\rangle = (|\uparrow\rangle - |\downarrow\rangle)/\sqrt{2}$ and $|e\rangle = (|\uparrow\rangle + |\downarrow\rangle)/\sqrt{2}$. In this basis, $\sigma_z = (|g\rangle\langle e| + |e\rangle\langle g|)$, and

$$H_{TLS} = \hbar\omega \hat{a}^\dagger \hat{a} + \frac{E_J}{2} (|e\rangle\langle e| - |g\rangle\langle e|) + \lambda \frac{\hat{a} + \hat{a}^\dagger}{2} + [-\frac{\lambda}{2}(\hat{a} + \hat{a}^\dagger) + 4E_c(n_g - 1/2)](|g\rangle\langle e| + |e\rangle\langle g|). \quad (\text{C1})$$

We can absorb the $\lambda \frac{\hat{a} + \hat{a}^\dagger}{2}$ term by a redefinition of the creation and annihilation operators, $\hat{a}' = \hat{a} + \frac{\lambda}{2\hbar\omega}$. In terms of these new operators, selecting n_g such that

$$\frac{\lambda^2}{2\hbar\omega} + 4E_c(n_g - 1/2) = 0, \quad (\text{C2})$$

we obtain

$$H_{TLS} = \hbar\omega \hat{a}'^\dagger \hat{a}' + \frac{E_J}{2} (|e\rangle\langle e| - |g\rangle\langle e|) - \frac{\lambda}{2} (\hat{a}' + \hat{a}'^\dagger) (|g\rangle\langle e| + |e\rangle\langle g|). \quad (\text{C3})$$

Let us consider the resonant limit $\hbar\omega \approx E_J$. In this case absorption of a photon exactly gives the excitation energy from $|g\rangle$ to $|e\rangle$. In this case, when the Rabi frequency is small compared to the excitation energy, $\lambda \ll \hbar\omega \approx E_J$, it is legitimate to neglect the counter rotating terms and obtain the Jaynes–Cummings Hamiltonian,

$$H_{TLS} = \hbar\omega \hat{a}'^\dagger \hat{a}' + \frac{E_J}{2} (|e\rangle\langle e| - |g\rangle\langle g|) - \frac{\lambda}{2} (\hat{a}'^\dagger |g\rangle\langle e| + \hat{a}' |e\rangle\langle g|). \quad (\text{C4})$$

The Rabi oscillations occurring when the creation and annihilation operators are replaced by a classical field, are strongly modified when one considers a mesoscopic coherent state with a not-too-large value of n_{ph} . This is the model studied in [43]

With an initial state $|g\rangle \otimes |\alpha\rangle$ with $|\alpha\rangle = \sum_{n=0}^{\infty} c_n |n\rangle$ with $c_n = \exp(-|\alpha|^2/2) \alpha^n / \sqrt{n!}$, let us follow [43] and compute the probability to find the excited state at time t . Let us set the resonant condition $\hbar\omega = E_J$. Then the eigenstates are $|g, 0\rangle$ and

$$|\pm\rangle_n = (|g, n\rangle \pm |e, n-1\rangle) / \sqrt{2}. \quad (\text{C5})$$

We can expand the initial state in eigenstates,

$$|\Psi(0)\rangle = |g\rangle \otimes |\alpha\rangle = c_0 |g, 0\rangle + \sum_{n=1}^{\infty} c_n \frac{|+\rangle_n + |-\rangle_n}{\sqrt{2}}. \quad (\text{C6})$$

Therefore

$$\langle e | \Psi(t) \rangle = \sum_{n=1}^{\infty} c_n \frac{e^{-iE_{|+\rangle_n} t/\hbar} - e^{-iE_{|-\rangle_n} t/\hbar}}{2}, \quad (\text{C7})$$

hence the time dependent excitation probability is given by [43]

$$P_e(t) = \sum_{n=1}^{\infty} c_n \sin^2 \frac{(E_{|+\rangle_n} - E_{|-\rangle_n})t}{2\hbar} = \sum_{n=1}^{\infty} c_n \sin^2 \frac{\lambda \sqrt{n} t}{2\hbar}, \quad (\text{C8})$$

which displays collapse and revivals as seen in Fig. 9. Suppose first that we replace n by its average $\langle n \rangle = \sum_{n=0}^{\infty} c_n^2 n = n_{ph}$. The resulting Rabi period T_R is defined by $\pi = \frac{\lambda \sqrt{n_{ph} T_R}}{2}$. In Fig. 9 we plot $P_e(t)$ in these units for $n_{ph} = 13.4$ as in

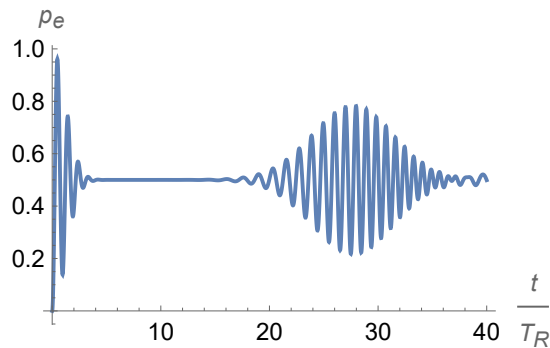


FIG. 9. Collapse and revival of Rabi oscillations according to Eq. (C8).

[43]. We see first a collapse of the oscillations due to the dispersion of frequencies. The dispersion of frequencies turns out to be of order λ . Therefore $t_{collapse} = 1/\lambda$. So there are $\sim \sqrt{n_{ph}}$ oscillation before the decay [43]. Interestingly, then there is a revival. By setting the relative phase of two neighboring frequencies to be 2π ,

$$2\pi = \frac{\lambda\sqrt{n+1}t_{revival}}{2} - \frac{\lambda\sqrt{n}t_{revival}}{2}, \quad (C9)$$

we obtain

$$t_{revival} = \frac{\pi\sqrt{n_{ph}}}{\lambda}. \quad (C10)$$

So there are $\sim n_{ph}$ oscillations till recovery [43].

-
- [1] M. Scandi, H. J. D. Miller, J. Anders, and M. Perarnau-Llobet, Quantum work statistics close to equilibrium, *Phys. Rev. Res.* **2**, 023377 (2020).
 - [2] R. Dorner, J. Goold, C. Cormick, M. Paternostro, and V. Vedral, Emergent thermodynamics in a quenched quantum many-body system, *Phys. Rev. Lett.* **109**, 160601 (2012).
 - [3] L. Fusco, S. Pigeon, T. J. G. Apollaro, A. Xuereb, L. Mazzola, M. Campisi, A. Ferraro, M. Paternostro, and G. De Chiara, Assessing the nonequilibrium thermodynamics in a quenched quantum many-body system via single projective measurements, *Phys. Rev. X* **4**, 031029 (2014).
 - [4] J. Goold, F. Plastina, A. Gambassi, and A. Silva, The role of quantum work statistics in many-body physics, *Thermodynamics in the Quantum Regime: Fundamental Aspects and New Directions*, 317 (2018).
 - [5] S. Suomela, P. Solinas, J. P. Pekola, J. Ankerhold, and T. Ala-Nissila, Moments of work in the two-point measurement protocol for a driven open quantum system, *Phys. Rev. B* **90**, 094304 (2014).
 - [6] A. Silva, Statistics of the work done on a quantum critical system by quenching a control parameter, *Physical review letters* **101**, 120603 (2008).
 - [7] E. Mascarenhas, H. Bragança, R. Dorner, M. França Santos, V. Vedral, K. Modi, and J. Goold, Work and quantum phase transitions: Quantum latency, *Phys. Rev. E* **89**, 062103 (2014).
 - [8] K. Zawadzki, R. M. Serra, and I. D'Amico, Work-distribution quantumness and irreversibility when crossing a quantum phase transition in finite time, *Phys. Rev. Res.* **2**, 033167 (2020).
 - [9] Z. Fei, N. Freitas, V. Cavina, H. Quan, and M. Esposito, Work statistics across a quantum phase transition, *Phys. Rev. Lett.* **124**, 170603 (2020).
 - [10] D. Rossini and E. Vicari, Coherent and dissipative dynamics at quantum phase transitions, *Phys. Rep.* **936**, 1 (2021).
 - [11] T. Van Vu and K. Saito, Finite-time quantum landauer principle and quantum coherence, *Phys. Rev. Lett.* **128**, 010602 (2022).
 - [12] H. J. D. Miller, G. Guarnieri, M. T. Mitchison, and J. Goold, Quantum fluctuations hinder finite-time information erasure near the landauer limit, *Phys. Rev. Lett.* **125**, 160602 (2020).
 - [13] C. Elouard, D. Herrera-Martí, B. Huard, and A. Auffèves, Extracting work from quantum measurement in maxwell's demon engines, *Phys. Rev. Lett.* **118**, 260603 (2017).
 - [14] N. Cottet, S. Jezouin, L. Bretheau, P. Campagne-Ibarcq, Q. Ficheux, J. Anders, A. Auffèves, R. Azouit, P. Rouchon, and B. Huard, Observing a quantum maxwell demon at work, *Proc. Nat. Acad. Sci.* **114**, 7561 (2017).
 - [15] C. Jarzynski, Nonequilibrium equality for free energy dif-

- ferences, *Phys. Rev. Lett.* **78**, 2690 (1997).
- [16] G. E. Crooks, Entropy production fluctuation theorem and the nonequilibrium work relation for free energy differences, *Phys. Rev. E* **60**, 2721 (1999).
- [17] D. Mandal and C. Jarzynski, Analysis of slow transitions between nonequilibrium steady states, *J. Stat. Mech.* **2016**, 063204 (2016).
- [18] H. J. D. Miller, M. Scandi, J. Anders, and M. Perarnau-Llobet, Work fluctuations in slow processes: Quantum signatures and optimal control, *Phys. Rev. Lett.* **123**, 230603 (2019).
- [19] A. Smith, Y. Lu, S. An, X. Zhang, J.-N. Zhang, Z. Gong, H. Quan, C. Jarzynski, and K. Kim, Verification of the quantum nonequilibrium work relation in the presence of decoherence, *New Jour. Phys.* **20**, 013008 (2018).
- [20] O.-P. Saira, Y. Yoon, T. Tanttu, M. Möttönen, D. Averin, and J. P. Pekola, Test of the jarzynski and crooks fluctuation relations in an electronic system, *Phys. Rev. Lett.* **109**, 180601 (2012).
- [21] J. Koski, T. Sagawa, O. Saira, Y. Yoon, A. Kutvonen, P. Solinas, M. Möttönen, T. Ala-Nissila, and J. Pekola, Distribution of entropy production in a single-electron box, *Nat. Phys.* **9**, 644 (2013).
- [22] A. Hofmann, V. F. Maisi, C. Rössler, J. Basset, T. Krähenmann, P. Märki, T. Ihn, K. Ensslin, C. Reichl, and W. Wegscheider, Equilibrium free energy measurement of a confined electron driven out of equilibrium, *Phys. Rev. B* **93**, 035425 (2016).
- [23] A. Hofmann, V. F. Maisi, J. Basset, C. Reichl, W. Wegscheider, T. Ihn, K. Ensslin, and C. Jarzynski, Heat dissipation and fluctuations in a driven quantum dot, *Phys. Stat. Sol. B* **254**, 1600546 (2017).
- [24] D. Barker, M. Scandi, S. Lehmann, C. Thelander, K. A. Dick, M. Perarnau-Llobet, and V. F. Maisi, Experimental verification of the work fluctuation-dissipation relation for information-to-work conversion, *Phys. Rev. Lett.* **128**, 040602 (2022).
- [25] J. P. Pekola, P. Solinas, A. Shnirman, and D. Averin, Calorimetric measurement of work in a quantum system, *N. J. Phys.* **15**, 115006 (2013).
- [26] P. Talkner, E. Lutz, and P. Hänggi, Fluctuation theorems: Work is not an observable, *Phys. Rev. E* **75**, 050102 (2007).
- [27] R. Dorner, S. R. Clark, L. Heaney, R. Fazio, J. Goold, and V. Vedral, Extracting quantum work statistics and fluctuation theorems by single-qubit interferometry, *Phys. Rev. Lett.* **110**, 230601 (2013).
- [28] L. Mazzola, G. De Chiara, and M. Paternostro, Measuring the characteristic function of the work distribution, *Phys. Rev. Lett.* **110**, 230602 (2013).
- [29] D. Cohen and Y. Imry, Straightforward quantum-mechanical derivation of the crooks fluctuation theorem and the jarzynski equality, *Phys. Rev. E* **86**, 011111 (2012).
- [30] J. Åberg, Catalytic coherence, *Phys. Rev. Lett* **113**, 150402 (2014).
- [31] K. Korzekwa, M. Lostaglio, J. Oppenheim, and D. Jennings, The extraction of work from quantum coherence, *N. J. Phys.* **18**, 023045 (2016).
- [32] M. Lobejko, Work and fluctuations: Coherent vs. incoherent ergotropy extraction, *Quantum* **6**, 762 (2022).
- [33] P. Skrzypczyk, A. J. Short, and S. Popescu, Work extraction and thermodynamics for individual quantum systems, *Nature communications* **5**, 4185 (2014).
- [34] T. Biswas, M. Lobejko, P. Mazurek, K. Jałowiecki, and M. Horodecki, Extraction of ergotropy: Free energy bound and application to open cycle engines, *Quantum* **6**, 841 (2022).
- [35] D. Gelbwaser-Klimovsky, R. Alicki, and G. Kurizki, Work and energy gain of heat-pumped quantized amplifiers, *Euro. Lett.* **103**, 60005 (2013).
- [36] J. Monsel, C. Elouard, and A. Auffèves, An autonomous quantum machine to measure the thermodynamic arrow of time, *npj Quantum Information* **4**, 59 (2018).
- [37] F. Campaioli, S. Gherardini, J. Q. Quach, M. Polini, and G. M. Andolina, Colloquium: quantum batteries, *Rev. Mod. Phys.* **96**, 031001 (2024).
- [38] A. Levy, L. Diósi, and R. Kosloff, Quantum flywheel, *Phys. Rev. A* **93**, 052119 (2016).
- [39] W. S. Martins, F. Carollo, W. Li, K. Brandner, and I. Lesanovsky, Rydberg-ion flywheel for quantum work storage, *Phys. Rev. A* **108**, L050201 (2023).
- [40] D. von Lindenfels, O. Gräß, C. T. Schmiegelow, V. Kaushal, J. Schulz, M. T. Mitchison, J. Goold, F. Schmidt-Kaler, and U. G. Poschinger, Spin heat engine coupled to a harmonic-oscillator flywheel, *Phys. Rev. Lett.* **123**, 080602 (2019).
- [41] C. Han, D. Cohen, and E. Sela, Quantum limitation on experimental testing of nonequilibrium fluctuation theorems, *Phys. Rev. B* **110**, 115153 (2024).
- [42] J. Koch, T. M. Yu, J. Gambetta, A. A. Houck, D. I. Schuster, J. Majer, A. Blais, M. H. Devoret, S. M. Girvin, and R. J. Schoelkopf, Charge-insensitive qubit design derived from the cooper pair box, *Phys. Rev. A* **76**, 042319 (2007).
- [43] T. Meunier, S. Gleyzes, P. Maioli, A. Auffèves, G. Nogues, M. Brune, J. Raimond, and S. Haroche, Rabi oscillations revival induced by time reversal: a test of mesoscopic quantum coherence, *Phys. Rev. Lett.* **94**, 010401 (2005).
- [44] S. Suomela, P. Solinas, J. P. Pekola, J. Ankerhold, and T. Ala-Nissila, Moments of work in the two-point measurement protocol for a driven open quantum system, *Phys. Rev. B* **90**, 094304 (2014).
- [45] C. Han, Y. Meir, and E. Sela, Realistic protocol to measure entanglement at finite temperatures, *Phys. Rev. Lett.* **130**, 136201 (2023).
- [46] M. Goldstein, M. H. Devoret, M. Houzet, and L. I. Glazman, Inelastic microwave photon scattering off a quantum impurity? format? in a josephson-junction array, *Phys. Rev. Lett.* **110**, 017002 (2013).
- [47] T. Frey, P. Leek, M. Beck, A. Blais, T. Ihn, K. Ensslin, and A. Wallraff, Dipole coupling of a double quantum dot to a microwave resonator, *Phys. Rev. Lett.* **108**, 046807 (2012).
- [48] K. D. Petersson, L. W. McFaul, M. D. Schroer, M. Jung, J. M. Taylor, A. A. Houck, and J. R. Petta, Circuit quantum electrodynamics with a spin qubit, *Nature* **490**, 380–383 (2012).
- [49] M. R. Delbecq, V. Schmitt, F. D. Parmentier, N. Roch, J. J. Viennot, G. Fève, B. Huard, C. Mora, A. Cottet, and T. Kontos, Coupling a quantum dot, fermionic leads, and a microwave cavity on a chip, *Phys. Rev. Lett.* **107**, 256804 (2011).
- [50] H. Toida, T. Nakajima, and S. Komiyama, Vacuum rabi splitting in a semiconductor circuit qed system, *Phys. Rev. Lett.* **110**, 066802 (2013).
- [51] L. E. Bruhat, T. Cubaynes, J. J. Viennot, M. C. Darti-

- ailh, M. M. Desjardins, A. Cottet, and T. Kontos, Circuit qed with a quantum-dot charge qubit dressed by cooper pairs, *Phys. Rev. B* **98** (2018).
- [52] X. Mi, J. V. Cady, D. M. Zajac, P. W. Deelman, and J. R. Petta, Strong coupling of a single electron in silicon to a microwave photon, *Science* **355**, 156–158 (2017).
- [53] A. Stockklauser, P. Scarlino, J. V. Koski, S. Gasparinetti, C. K. Andersen, C. Reichl, W. Wegscheider, T. Ihn, K. Ensslin, and A. Wallraff, Strong coupling cavity qed with gate-defined double quantum dots enabled by a high impedance resonator, *Phys. Rev. X* **7**, 011030 (2017).
- [54] Z. Iftikhar, S. Jezouin, A. Anthore, U. Gennser, F. Parmentier, A. Cavanna, and F. Pierre, Two-channel kondo effect and renormalization flow with macroscopic quantum charge states, *Nature* **526**, 233 (2015); A. K. Mitchell, L. Landau, L. Fritz, and E. Sela, Universality and scaling in a charge two-channel kondo device, *Phys. Rev. Lett.* **116**, 157202 (2016).
- [55] Z. Iftikhar, A. Anthore, A. Mitchell, F. Parmentier, U. Gennser, A. Ouerghi, A. Cavanna, C. Mora, P. Simon, and F. Pierre, Tunable quantum criticality and superballistic transport in a “charge” kondo circuit, *Science* **360**, 1315 (2018).
- [56] C. Piquard, P. Glidic, C. Han, A. Aassime, A. Cavanna, U. Gennser, Y. Meir, E. Sela, A. Anthore, and F. Pierre, Observing the universal screening of a kondo impurity, *Nature Communications* **14**, 7263 (2023).
- [57] A. K. Mitchell, L. A. Landau, L. Fritz, and E. Sela, Universality and scaling in a charge two-channel kondo device, *Phys. Rev. Lett.* **116**, 157202 (2016).
- [58] C. Han, Z. Iftikhar, Y. Kleeorin, A. Anthore, F. Pierre, Y. Meir, A. K. Mitchell, and E. Sela, Fractional entropy of multichannel kondo systems from conductance-charge relations, *Phys. Rev. Lett.* **128**, 146803 (2022).
- [59] W. Pouse, L. Peeters, C. L. Hsueh, U. Gennser, A. Cavanna, M. A. Kastner, A. K. Mitchell, and D. Goldhaber-Gordon, Quantum simulation of an exotic quantum critical point in a two-site charge kondo circuit, *Nature Physics* **19**, 492 (2023); D. Karki, E. Boulat, W. Pouse, D. Goldhaber-Gordon, A. K. Mitchell, and C. Mora, Z₃ parafermion in the double charge kondo model, *Phys. Rev. Lett.* **130**, 146201 (2023).
- [60] Z. Ma, A. K. Mitchell, and E. Sela, Quantum work statistics across a critical point: full crossover from sudden quench to the adiabatic limit, arXiv preprint arXiv:2502.01601 (2025).